JGR Atmospheres

RESEARCH ARTICLE
10.1029/2023JD039158

# Characteristics of Daytime-And-Nighttime AOD Differences Over China: A Perspective From CALIOP Satellite Observations and GEOS-Chem Model Simulations

**Xiaodong Jiang[1], Yi Wang[1], Lunche Wang[1,2], Minghui Tao[1], Jun Wang[3,4], Meng Zhou[4,5,6], Xuehui Bai[1], and Lu Gui[1]**

[1]Hubei Key Laboratory of Regional Ecology and Environmental Change, School of Geography and Information Engineering, China University of Geosciences, Wuhan, China, [2]Hubei Luojia Laboratory, Wuhan, China, [3]Department of Chemical and Biochemical Engineering, The University of Iowa, Iowa City, IA, USA, [4]Center for Global and Regional Environmental Research, The University of Iowa, Iowa City, IA, USA, [5]Interdisciplinary Graduate Program in Geo-Informatics, The University of Iowa, Iowa City, IA, USA, [6]Now at Goddard Earth Sciences Technology and Research, University of Maryland, Baltimore County, Baltimore, MD, USA

**Key Points:**

- CALIOP observes that Aerosol Optical Depth (AOD) is larger in the nighttime than during the daytime over eastern China
- Larger nighttime AOD is mainly due to greater hygroscopic growth related to larger relative humidity at night in lower troposphere
- The CALIOP detection limit difference between daytime and nighttime partly contributes to the larger nighttime AOD below 5 km

**Supporting Information:**

Supporting Information may be found in the online version of this article.

**Correspondence to:**

Y. Wang,
wangyi34@cug.edu.cn

**Citation:**

Jiang, X., Wang, Y., Wang, L., Tao, M., Wang, J., Zhou, M., et al. (2024). Characteristics of daytime-and-nighttime AOD differences over China: A perspective from CALIOP satellite observations and GEOS-Chem model simulations. *Journal of Geophysical Research: Atmospheres*, *129*, e2023JD039158. https://doi.org/10.1029/2023JD039158

Received 25 APR 2023
Accepted 28 MAR 2024



**Abstract** We use the GEOS-Chem chemistry transport model to quantify the factors in the diel discrepancy of Aerosol Optical Depth (AOD) retrieved from Cloud-Aerosol Lidar with Orthogonal Polarization (CALIOP) satellite observations over eastern China. The GEOS-Chem simulation reveals that the AOD below 1 km is 58.5% larger at night than during the daytime, which is comparable to the counterpart of 41.3% from CALIOP (v4.2). Model sensitivity simulations show that the diurnal variation in wind barely impacts the AOD difference between daytime and nighttime, and the increase in AOD at nighttime is primarily caused by the lower temperature at nighttime compared to daytime. Further simulations demonstrate that the low temperature at night increases AOD primarily by increasing relative humidity, and hence particle hygroscopic growth, while the effect of temperature on chemical rate barely influences AOD. CALIOP also observes that the absolute difference in AOD above 1 km between nighttime and daytime is 0.105, while the counterpart in GEOS-Chem simulations is −0.031. This contrast can be partly explained by the factor that the percentage of valid CALIOP retrievals below 5 km is 15%–20% greater at nighttime than in the daytime due to the CALIOP detection limit. Removing the detection limit impact decreases the difference in the CALIOP AOD above 1 km between nighttime and daytime to 0.073.

**Plain Language Summary** Aerosols are small particulates suspended in the atmosphere, having adverse impacts on human health, and modifying climate forcing. Satellite-based Aerosol Optical Depth (AOD), while often used as an observation-based indicator of air pollution at global and regional scale, contains not only information on aerosol dry mass concentrations but also information on aerosol optical properties that link mass to optical extinction. We found that satellite-based AOD at night is larger than that in the daytime over eastern China. The disparities cannot be explained by the difference in aerosol dry mass loading alone, and indeed, is primarily caused by larger relative humidity that in turn makes aerosol particle size larger and changes aerosol extinction efficiency via greater hygroscopic growth at night. As the space-borne lidar (CLAIOP) that is designed to measure both daytime and nighttime AOD was decommissioned in August 2023, this study not only reveals the diurnal variation in the relationship between AOD and aerosol dry mass concentrations but also underscores the emergent need and critical importance of nighttime AOD measurements from space for studying air quality and aerosol processes at regional to global scale.

## 1. Introduction

Aerosols exhibit diurnal variations (Balmes et al., 2021) due to differences in emissions (Crippa et al., 2020; Wang et al., 2004), meteorological conditions (Wang et al., 2006; Xu et al., 2019), and chemistry processes (Seinfeld & Pandis, 2016; Wang et al., 2020) between daytime and nighttime. Characterizing the spatial distribution of aerosols in the daytime as well as nighttime is important for investigating their impacts on global radiative forcing and human health. Aerosols alter the Earth's radiation budget directly by interacting with radiation and indirectly by changing cloud lifetime and microphysical properties (Haywood & Boucher, 2000; Myhre et al., 2013). These direct and indirect effects are not limited to solar shortwave radiation during the day but also affect terrestrial longwave radiation throughout the day and night (Gasparini et al., 2020; Jackson

et al., 2016). According to the Intergovernmental Panel on Climate Change (IPCC) Sixth Assessment Report (AR6), aerosols contribute 1.3 ± 0.7 W $m^{-2}$ to global effective radiative forcing (Smith et al., 2021). Apart from their impact on the radiation budget, aerosols near the Earth's surface also adversely affect human health. Aerosols with an aerodynamic diameter less than 2.5 μm ($PM_{2.5}$) can cause and exacerbate acute lower respiratory illness, cerebrovascular disease, ischemic heart disease, chronic obstructive pulmonary disease, and lung cancer (Burnett et al., 2014). It was estimated that $PM_{2.5}$ pollution caused ∼3 million premature deaths in 2010 worldwide, with ∼1.3 million occurring in China (Lelieveld et al., 2015). Despite the large diurnal variations in $PM_{2.5}$ concentrations (Fu et al., 2018), the $PM_{2.5}$ concentration data used for estimating premature deaths are obtained from model simulations or derived from daytime satellite-based Aerosol Optical Depth (AOD) retrievals, lacking observational information at nighttime (Lee et al., 2015; Lelieveld et al., 2015; Wei, Li, Lyapustin, et al., 2021).

Due to their wide spatial coverage, AOD data from satellite sensors such as Moderate Resolution Imaging Spectroradiometer (MODIS), Multi-angle Imaging Spectroradiometer (MISR), Visible Infrared Imaging Radiometer Suite (VIIRS), and Advanced Himawari Imager (AHI) have been used for estimating emissions (Petrenko et al., 2012; Xu et al., 2013; Ye et al., 2023), investigating radiative forcing (Ge et al., 2010; Jia et al., 2021; Ma et al., 2014; Xu et al., 2022), and deriving surface $PM_{2.5}$ concentrations (Wei et al., 2021a, 2021b; Wu et al., 2016; Yao et al., 2018; You et al., 2016). However, all these passive satellite sensors, except for VIIRS, measure only reflected sunlight radiance for retrieving AOD in the daytime. Although VIIRS measures reflected moonlight and city nighttime light in addition to reflected sunlight, research on using VIIRS to retrieve nighttime AOD or study urban air pollution is still in a preliminary stage (Meng et al., 2023; Wang et al., 2016; Zhang et al., 2023; Zhou et al., 2021), and there is no operational VIIRS nighttime AOD product.

Unlike passive satellite sensors, the active Cloud-Aerosol Lidar with Orthogonal Polarization (CALIOP) sensor on board the Cloud-Aerosol Lidar and Infrared Pathfinder Satellite Observation (CALIPSO) satellite measures the attenuated backscatter light beam, which is used to retrieve Extinction Coefficient (EC) profiles and consequently columnar AOD in both the daytime and nighttime. CALIOP daytime and nighttime AOD data have been compared at both global and regional scale. Previous research has shown that the global pattern of CALIOP AOD in the daytime is similar to that at nighttime (Kittaka et al., 2011; Ma et al., 2013; Winker et al., 2013), but the mean CALIOP AOD at nighttime is 17%–46% higher than that during the daytime over land (Ma et al., 2013; Winker et al., 2013). The factors in these large differences have not been investigated with rigor. At regional scale, the CALIOP data show that AOD at nighttime is larger than that in the daytime over eastern China (Gui et al., 2022; Huang et al., 2013) and the North China Plain (Xu et al., 2019). The larger nighttime AOD is ascribed to weaker convection and diffusion caused by lower temperature at night (Gui et al., 2022), greater hygroscopic growth of aerosols at low levels at nighttime than during the day (Xu et al., 2019), and undetected daytime low aerosol concentrations at high levels caused by solar radiation interference (Xu et al., 2019). In contrast, Su et al. (2020) found that CALIOP AOD is larger during the daytime than at night over northeastern China and hypothesized that this difference is caused by greater anthropogenic emissions during the day than at night.

Despite the previous research on the differences between daytime and nighttime CALIOP AOD, the primary drivers regulating these variations have not been quantified. All these studies focus on analyzing AOD and EC profile data from CALIOP or meteorological data from model simulations, but they lack the simulation of AOD diurnal variations. AOD is affected by many factors, including emissions, chemistry processes, transport, and hygroscopic growth; thus, it can be challenging to quantify the contributions without Chemistry Transport Model (CTM) simulations. We use the GEOS-Chem CTM to simulate the diurnal variations in AOD over China and quantify the factors in the daytime-and-nighttime AOD differences through sensitivity experiments. Section 2 introduces the data sets, CTM, experimental design, and data processing. Section 3 describes the results of CALIOP observations and GEOS-Chem simulations. Section 4 provides a discussion, while Section 5 presents conclusions.

## 2. Data and Method

### 2.1. CALIOP Data

In this study, we use CALIOP level-2 and level-3 aerosol EC profiles and AOD to investigate the differences in aerosol loading between daytime and nighttime. The CALIOP lidar onboard the CALIPSO satellite, launched on 28 April 2006, flies across the equator at ∼13:30 and ∼01:30 local time in the daytime and nighttime, respectively. CALIOP observes linear polarization backscatter at 532 nm and total backscatter at 1,064 nm, which can be used to retrieve aerosol EC profiles. We use CALIOP level-2 cloud-free aerosol profile product (version 4.2),

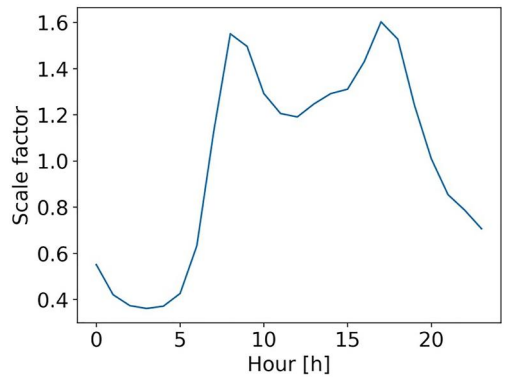


**Figure 1.** The spatial mean of the diurnal profile used for allocating daily anthropogenic NO emissions to every hour in the eastern China.

which includes aerosol EC profiles at 532 nm with a vertical resolution of 60 m ranging from −0.5 to 20 km in the troposphere for model evaluation and the comparison between daytime and nighttime aerosol characteristics. The CALIOP level-3 product is derived from the version 4.2 CALIOP level-2 aerosol profile product through quality control and regridding (Tackett et al., 2018). The level-3 cloud-free AOD has a horizontal resolution of $2° \times 5°$ and a temporal resolution of 1 month. As the CALIOP level-3 product is monthly mean data, it cannot be properly collocated with CTM simulations; level-3 data during 2007–2019 are only used for long-term analysis. It is worth noting that the daytime CALIOP measurements exhibit a lower Signal-Noise Ratio (SNR) compared to nighttime, due in part to factors like sunlight interference. As a result, some faint aerosol layers that may be detected during nighttime conditions are undetected in the daytime and thus classified as "clear air" (Kim et al., 2017). For these layers, aerosol extinction coefficient retrievals are not conducted. In the evaluation of climatological AOD characteristics setting EC values of "clear air" samples to zero lead to an underestimate. As there are more "clear air" samples in the daytime than at nighttime, this underestimation will be larger in the daytime than at nighttime. The impact of how to deal with "clear air" samples on the daytime-and-nighttime AOD difference is discussed in Section 4.1.

### 2.2. GEOS-Chem Model

GEOS-Chem is a global three-dimensional Chemistry Transport Model (CTM) with aerosol external mixing and hygroscopic growth implemented (Bey et al., 2001; Wang & Martin, 2007). In this study, we use GEOS-Chem version 13.3 driven by the Modern-Era Retrospective Analysis for Research and Applications (MERRA-2) (Gelaro et al., 2017) from NASA's Global Modeling and Assimilation Office to simulate species concentrations, EC, and AOD at an hourly temporal resolution, $2° \times 2.5°$ horizonal resolution, and 47 vertical layers from surface to 80 km for 2019 over China. The anthropogenic emission inventory used is the Community Emissions Data System version 2 (CEDSv2) (McDuffie et al., 2020) with a temporal resolution of 1 month, and are evenly allocated to every day. In GEOS-Chem, the daily anthropogenic emissions of all species are evenly allocated to every hour except for NO, whose hourly allocation is conducted according to the diurnal profile in Figure 1. Dust emissions are calculated online through the mineral dust entrainment and deposition (Fairlie et al., 2007; Zender et al., 2003) scheme at every 20-min time step.

Sulfate, nitrate, ammonium, fine mode sea salt, coarse mode sea salt, and parts of Black Carbon (BC) and Organic Carbon (OC) species are hygroscopic and can absorb water as Relative Humidity (RH) increases, and their scattering efficiency is enhanced accordingly (Wang et al., 2008). In GEOS-Chem, the species used to calculate AOD include sulfate, nitrate, ammonium, fine mode sea salt, coarse mode sea salt, BC, OC, and dust in four size bins. When relative humidity exceeds 0%, hygroscopic growth occurs, changing the optical property and size of aerosols and thus affecting AOD.

### 2.3. Meteorological Data

In addition to MERRA-2, we use three-dimensional temperature, specific humidity, and relative humidity data from Atmospheric InfraRed Sounder (AIRS), and ERA5 in this study. These data are used to evaluate the meteorological variables from MERRA-2. AIRS is a hyperspectral infrared spectrometer (Aumann et al., 2003) aboard the Aqua satellite, which passes over the equator at ∼13:30 and ∼01:30 local time in the daytime and nighttime, respectively. We use version 7 level-3 products (Tian et al., 2020) from AIRS, which have a 1°×1° horizontal resolution and a temporal resolution of 1 month. The AIRS temperature data spans 24 levels ranging from 1,000 to 1 hPa, while both relative humidity and specific humidity are available at 12 levels in the range of 1,000 to 100 hPa. ERA5 is the fifth-generation atmospheric product provided by the European Center for Medium-Range Weather Forecasts (Hersbach et al., 2020). Compared with its predecessor ERA-Interim, ERA5 employs a more advanced data assimilation scheme and a broader spectrum of data sources to calculate various atmospheric variables (Hersbach et al., 2020). In this study, we use ERA5 hourly data on pressure levels with a regular horizontal resolution of $0.25° \times 0.25°$ and 37 pressure levels from 1,000 to 1 hPa.

### 2.4. AERONET Data

Daytime and nighttime AOD measurements from the ground-based Aerosol Robotic Network (AERONET) are used. 532 nm AOD data are derived from 500 nm AOD and 675 nm AOD through logarithmic interpolation. Level 2.0 daytime AERONET AOD data are quality assured and are used in this study. Yet there is only level 1.5 rather than level 2.0 nighttime AERONET AOD data with provisional quality assurance, which means the level 1.5 data is not finalized and may change. There is a discussion of the result derived from AERNOET AOD measurements in Section 4.1.

### 2.5. Data Processing

To compare GEOS-Chem AOD with CALIOP level-2 retrievals, it is essential to apply CALIOP data quality control and sample GEOS-Chem data accordingly. Due to low instrument sensitivity near the Earth's surface, the CALIOP retrieving algorithm sometimes cannot detect the extinction coefficient profiles of the aerosol layers attached to the Earth's surface. Additionally, when the attenuated aerosol backscatter signal is smaller than $2–4 \times 10^{-4}$ $km^{-1}sr^{-1}$, CALIOP may lose its detection capability (Huang et al., 2013; Winker et al., 2009). We follow Winker et al. (2013) and NASA (2023c) to conduct quality control for CALIOP Level-2 data with these consecutive steps.

1. The cloud aerosol discrimination score should be within −100 to −20.
2. Extinction coefficients with Extinction_QC flags other than 0 or 1 are excluded, along with all data points below them.
3. Extinction coefficients with a profile uncertainty of 99.9 $km^{-1}$ are rejected, as well as all data below them.
4. Data that are within 60 m of the ground are rejected.
5. We remove all EC samples with cloud layer fraction larger than 97%, along with the samples below the rejected ones (NASA, 2023c).
6. For samples that are classified as "clear air" and above 250 m of the ground, these values are assumed to be 0.0 $km^{-1}$.
7. Samples that are classified as "clear air" and within 250 m of the ground are rejected.

After CALIOP data quality control, GEOS-Chem extinction coefficients data are sampled according to corresponding CALIOP retrievals, and the CALIOP retrievals are averaged to the $2° \times 2.5°$ GEOS-Chem horizonal grids. Hence GEOS-Chem and CALIOP data are spatially and temporally collocated for comparison. Only extinction coefficients below 12 km are vertically aggregated to calculate AOD.

### 2.6. Experimental Design

To quantify the contributions of various factors in the AOD difference between daytime and nighttime, we conduct four GEOS-Chem simulation experiments for 2019, which are summarized in Table 1. The first simulation (CONTROL) serves as a base experiment and is used for comparison with others. The second experiment ($TEMP_{all}$) exams the impact of temperature on aqueous-phase oxidation of $SO_2$ by $O_3$ and $H_2O_2$ in clouds to form sulfate and relative humidity related to aerosol hygroscopic growth by replacing nighttime temperature with daytime temperature. The MERRA-2 temperature data has a 3-hr temporal resolution starting from 02 hr every day, so the temperature at nighttime (20 hr, 23 hr, 02 hr, and 05 hr local time) is replaced by that in the daytime (08 hr, 11 hr, 14 hr, and 17 hr) in the simulation. To separate the impact of temperature on aerosol hygroscopic growth, the third experiment ($TEMP_{rh}$) only replaces the nighttime temperature used for calculating the relative humidity for aerosol hygroscopic growth with the daytime temperature. The fourth experiment (WIND) is designed to show how transport affects the daytime-and-nighttime AOD differences; we replace the nighttime wind with the daytime wind.

## 3. Results

### 3.1. CALIOP Daytime-And-Nighttime AOD Differences

CALIOP level-3 daytime and nighttime AOD over China during 2007–2019 is shown in Figure 2. Large CALIOP AOD exists over eastern China and the southern part of Xinjiang Province during both the daytime (Figure 2a) and nighttime (Figure 2b). The large AOD over eastern China is primarily due to anthropogenic emissions (Zheng et al., 2018), while dust aerosol is the major contributor to the large AOD over the southern part of Xinjiang

**Table 1**
*Experimental Design for Quantifying the Contribution of Various Factors to Daytime-And-Nighttime AOD Differences for 2019*

| Name | Description | Purpose |
|---|---|---|
| CONTROL | GEOS-Chem default setting. | Base experiment for comparison. |
| $TEMP_{all}$ | Replace the nighttime temperature with daytime temperature. | Explore the impact of the temperature variation on the daytime-and-nighttime AOD differences. |
| $TEMP_{rh}$ | The relative humidity used for aerosol hydroscopic growth during the nighttime is calculated using the daytime temperature. | Explore the impact of aerosol hydroscopic growth caused by the temperature variation on the daytime-and-nighttime AOD differences. |
| WIND | Replace the nighttime wind with daytime wind. | Explore the impact of transport on the daytime-and-nighttime AOD differences. |

Province (Liu et al., 2021). In general, the CALIOP AOD at nighttime is comparable to in the daytime over the southern part of Xinjiang Province, while it is larger than the daytime AOD over eastern China (Figures 2a and 2b). Considering that both the AOD and the daytime-and-nighttime difference are large over eastern China, we select 102°E to 120°E and 22°N to 40°N (the boxes in Figure 2) as our study region. Although CALIOP AOD is more than 100% larger at nighttime than in the daytime over Tibet, we exclude it from our study region as AOD is relatively small there.

Figure 3 illustrates the yearly absolute and relative CALIOP level-3 AOD differences between nighttime and daytime over eastern China (the boxes in Figure 2) from 2007 to 2019. It is evident that CALIOP AOD at nighttime is consistently larger than that during the daytime each year, with the smallest and largest absolute differences of 0.079 and 0.168, respectively, in 2010 and 2012. Meanwhile, the largest relative difference of 37.8% is observed in 2019. We choose this year for the GEOS-Chem simulations to investigate to why CALIOP AOD is larger at nighttime than during the daytime.

### 3.2. GEOS-Chem Simulation

#### 3.2.1. Model Evaluation

To investigate whether GEOS-Chem simulations can capture the AOD diurnal variation, we evaluate GEOS-Chem AOD and extinction coefficient profile simulations against the CALIOP level-2 product. Figures 4a and 4b show EC profiles in the vertical range of 0.2–5 km from CALIOP observations and the CONTROL simulation over eastern China (the boxes in Figure 2) in 2019 at daytime and nighttime, respectively. CONTROL captures well the characteristics that annual mean EC decreases with height at nighttime (Figure 4b). Regarding daytime, CONTROL shows an EC peak at 1.2 km with declining EC from this point to both surface and high layers while CALIOP observes that EC decreases with height. Although this modeled peak is a straightforward consequence of thermodynamics within the mixed layer, whether it shows in CALIOP observation is spatially and temporally dependent (Sect. S1 in Supporting Information S1). Figure 4c is a Taylor diagram (Taylor, 2001; Sect. S2 in Supporting Information S1) that shows CONTROL performs better at nighttime than daytime in terms of annual and seasonal EC profiles. Despite the performance difference between daytime and nighttime, CONTROL still capture the characteristic that AOD at nighttime is larger than that at daytime.

#### 3.2.2. Sensitivity Analysis

Figure 5 shows the daytime and nighttime AOD from the CALIOP level-2 products, CONTROL, $TEMP_{rh}$, and WIND for 2019. In eastern China (the boxes in Figure 2), the CALIOP mean AOD at nighttime (Figure 5b) is 0.488, which is 51.9% larger than the mean AOD of 0.321 in the daytime (Table 2). Meanwhile, although the relative difference in AOD between nighttime and daytime is only 8.9% in the CONTROL simulation (Figure 5h and Table 2), it does capture the phenomenon that AOD is higher at nighttime than in the daytime. Moreover, for aerosols below 1 km, the relative AOD difference between nighttime and daytime from CONTROL is 58.5%, which is comparable to 41.3% from CALIOP (Figure S3 in Supporting Information S1). As only nighttime meteorological data are replaced in $TEMP_{rh}$ and WIND, the differences in daytime AOD among all the simulations (CONTROL, $TEMP_{rh}$, and WIND) are relatively small (the first column of Figure 5 and Table 2). The nighttime AOD from $TEMP_{rh}$ is 8.7% lower than that from CONTROL (Figures 5f and 5j and Table 2). Such a decline in nighttime AOD leads the relative difference between nighttime and daytime changes from 8.9% in CONTROL to −4.5% in $TEMP_{rh}$ (Table 2). This indicates that the diel temperature variation plays a significant role in the phenomenon that AOD is higher at nighttime than during the daytime through large aerosol hygroscopic growth due to the high relative humidity caused by low temperature. Meanwhile, the diel temperature difference places a very small impact on the chemical processes (Section S4 in Supporting Information S1). Regarding the impact of transport, the comparison between CONTROL and WIND shows that wind barely contributes to the AOD difference between nighttime and daytime.

The daytime and nighttime EC profiles from CALIOP, CONTROL, $TEMP_{rh}$, and WIND over eastern China (the boxes in Figure 2) in 2019 are shown in Figure 6. Evidently, all the simulations generally capture the observed decrease trends in ECs with altitude at both daytime and nighttime (Figure 6) although a peak at daytime appearing at 1.2 ∼ 1.6 km in all the simulations is not shown in the CALIOP observation. CALIOP observes higher ECs at night compared to daytime below ∼5 km, with negligible differences above this altitude (Figure 6a). The EC profiles from the CONTROL simulation show the transitional height is at 1 km and ECs are

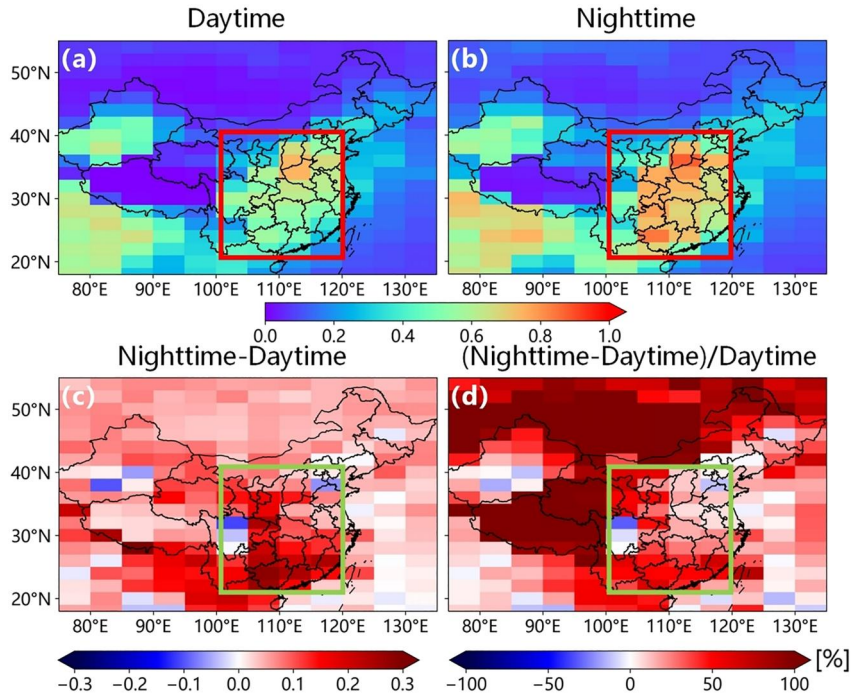


**Figure 2.** Daytime (a) and nighttime (b) CALIOP level-3 mean AOD distribution from 2007 to 2019. (c) and (d) are the absolute and relative differences between nighttime and daytime, respectively. The boxes (102°E to 120°E and 22°N to 40°N) in the panels are the study region (eastern China) of the research.

even a little higher at daytime than that at nighttime from 1.2 to 3 km (Figure 6b). Compared with CONTROL and CALIOP, the difference in EC between nighttime and daytime from $TEMP_{rh}$ is smaller below ~0.8 km, and EC in the nighttime is even a little smaller than that in the daytime above it. The extinction coefficient profiles throughout daytime and nighttime from $TEMP_{all}$ and $TEMP_{rh}$ are similar (Figure S5 in Supporting Information S1). This suggests that the nighttime AOD enhancement, attributed to hygroscopic growth due to low temperature at nighttime predominantly exists below 1 km. Furthermore, in the CONTROL run, if hygroscopic growth is not included in the post-processing computation of extinction coefficients, the AOD at nighttime drops to 0.242, which is smaller than the daytime AOD of 0.247. This also supports that the hygroscopic growth is essential in the larger nighttime AOD. The difference in ECs between CONTROL and WIND throughout daytime and nighttime is inconsequential, which means the diurnal variation in horizontal transport barely contribute to the AOD difference between nighttime and daytime. The disparities in AOD above 1 km between CALIOP and GEOS-Chem is discussed in Section 4.

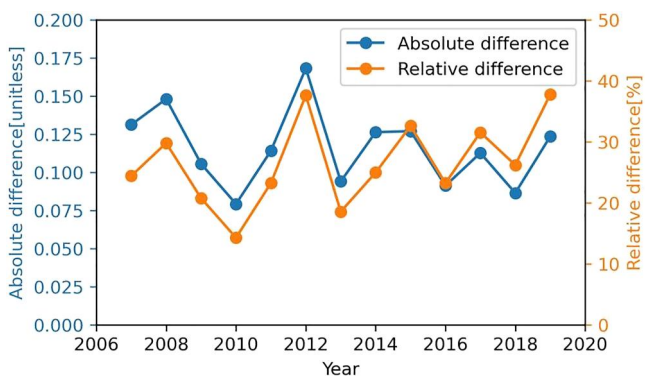


**Figure 3.** The yearly relative (orange line) and absolute (blue line) CALIOP level-3 AOD differences between nighttime and daytime over eastern China (boxes in Figure 2) during 2007–2019.

### 3.2.3. Relative Humidity Diurnal Variations

As the GEOS-Chem simulations show that large hygroscopic growth is the primary factor in the large nighttime AOD, we further validate and analyze the parameters related to relative humidity. Figure 7 shows the mean temperature, specific humidity, and relative humidity profiles at both daytime and nighttime over eastern China (the boxes in Figure 2) in 2019 from AIRS, MERRA-2 (GEOS-Chem), and ERA5. All three data sets show a decrease in temperature with altitude in both daytime and nighttime. AIRS observes that the temperature below ~2 km is lower at nighttime than in the daytime (Figure 7a), and the temperature difference decreases with altitude, with the daytime and nighttime temperature profiles almost coinciding above ~2 km. Both ERA5 (Figure 7b) and MERRA-2 (Figure 7c) capture these characteristics observed by AIRS (Figure 7a). Below 1.5 km, the specific humidity relative differences between nighttime and daytime are −1.10%, 0.12%, and

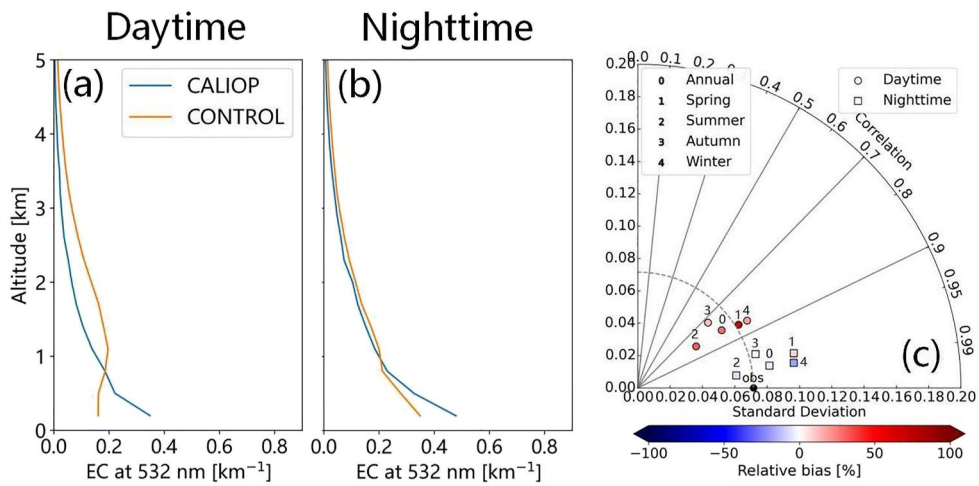


**Figure 4.** Extinction Coefficient (EC) profiles at 532 nm over eastern China (boxes in Figure 2) in daytime (a) and nighttime (b) in 2019. (c) is a Taylor diagram for evaluating the GEOS-Chem simulations with the CALIOP observations for daytime and nighttime.

−0.95% from AIRS, ERA5, and MERRA-2, respectively (Figures 7d–7f). The relative humidity profiles from the three data sets show that the relative humidity at nighttime is greater than that during the daytime below ∼1.5 km and the difference is larger at lower altitude (Figures 7g–7i). AIRS observes that relative humidity generally decreases with altitude at nighttime (Figure 7g). However, during the daytime the relative humidity increases with altitude, reaching a peak before decreasing again (Figure 7g). Both AIRS (Figure 7g) and MERRA-2 (Figure 7i) exhibit their highest relative humidity levels at approximately 1.5 km above sea level, while ERA5 (Figure 7h) peaks at ∼2 km. Above 2 km, both MERRA-2 (Figure 7i) and ERA5 (Figure 7h) show a minimal difference in relative humidity between daytime and nighttime, with the profiles nearly overlapping. In contrast, AIRS data (Figure 7g) show that daytime relative humidity is slightly greater than nighttime relative humidity between 2 and 4 km. Therefore, we conclude that the increased nighttime relative humidity can be attributed to a lower temperature, resulting in lower saturation water vapor pressure.

### 3.2.4. Species Diurnal and Vertical Variations

Figure 8 shows the diurnal variations in speciated AOD and dry mass in eastern China (the boxes in Figure 2) during 2019 from the CONTROL simulation. We use 2 a.m. and 2 p.m. to represent nighttime and daytime, respectively. The total AOD increases from 00 to 05 hr, decreases until reaching a low point at 15 hr, and then increases again. At 02 hr, the total AOD is 7.2% larger than that at 14 hr, whereas the total dry mass at 02 hr is only 2.6% larger than that at 14 hr. This indicates that hygroscopic growth is the primary factor responsible for the high nighttime AOD, and the impact of the diurnal variation of dust emissions is negligible (Figure 8). The sulfate-nitrate-ammonium (SNA) optical depth accounts for 62.2% of the total AOD. The SNA Optical Depth (OD) at 02 hr is 8.9% larger than that at 14 hr although the SNA mass is only 2.5% larger. Since the SNA has the largest contribution to total AOD and shows the largest diurnal variation, we further investigate the vertical profiles of SNA EC, dry mass concentration, radius growth factor (ratio of the wet aerosol effective radius to the dry aerosol effective radius), and extinction efficiency scale factor (ratio of the wet aerosol extinction efficiency to the dry aerosol extinction efficiency), which are the variables determining AOD (Sect. S5 in Supporting Information S1). Figure 9a shows that SNA EC from CONTROL is larger at nighttime than that at daytime below 1.5 km, but is a little smaller at nighttime than that at daytime at from 1.5 to 3 km. Although the pattern of dry mass profile (Figure 9b) is similar as that of EC (Figure 9b), the relative difference in EC below 1.5 km between nighttime and daytime is 61.7%, which is much larger than the relative difference in dry mass (25.4%). The patterns of SNA extinction efficiency scale factor profiles (Figure 9c) and the square of SNA radius growth factor profiles resonate the pattern of MERRA-2 relative humidity profile (Figure 7i) with increasingly larger values at nighttime than in the daytime toward lower altitude below ∼1.5 km. Although the larger SNA dry mass concentration at nighttime than that at daytime (Figures 8 and 9b) partly contributes to the diel SNA AOD difference (Figure 9b), SNA

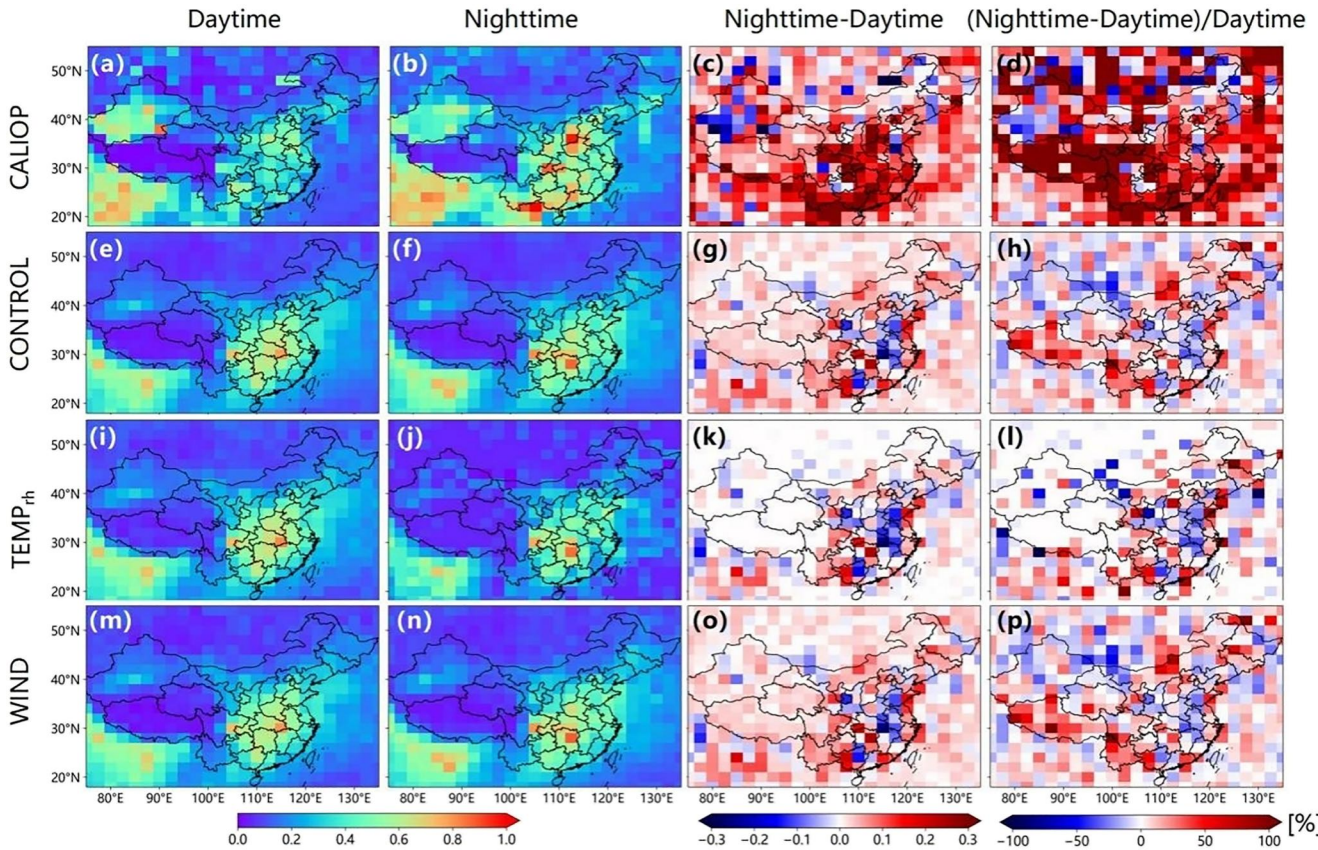


**Figure 5.** The daytime (first column) and nighttime (second column) AOD, and the absolute (third column) and relative (fourth column) AOD differences between nighttime and daytime in 2019 from CALIOP (first row), CONTROL (second row), TEMP$_{rh}$ (3rd row), and WIND (fourth row).

extinction efficiency scale factor and SNA radius growth factor are much larger and therefore a greater factor at nighttime than that at daytime play a more important role (Figures 9c and 9d).

## 4. Discussion

This study has quantified the factors in the difference in CALIOP AOD between nighttime and daytime through sensitivity analysis based on GEOS-Chem simulations. However, the impacts of CALIOP retrieval uncertainty, and diurnal variations in emissions on our findings should be discussed.

### 4.1. CALIOP Detection Limit and Uncertainty

In the CALIOP EC product, EC retrieval is not conducted for any layer that is classified as "clear air". Figure 10a shows that the extinction coefficient retrieval ability starts to diminish from 0.3 km upwards at both daytime and nighttime. Additionally, the percentage of valid retrievals at nighttime is 15%–20% more than that in the daytime from 0.3 to 5 km, and the difference decreases above 5 km. Thus, the impact of the variation in CALIOP SNR on the daytime-and-nighttime AOD difference exists at both low levels (below 1 km) and high levels (1–5 km).

On the one hand, as there are more samples classified as "clear air" in the daytime than at nighttime, setting the EC of these samples to 0 in this study can introduce a larger artificial underestimate of AOD in the daytime than at nighttime. This artificial difference in underestimation could partly explain that AOD is larger at nighttime than in the daytime. Meanwhile, the GEOS-

**Table 2**
*The Mean AOD Over Eastern China (Boxes in Figure 2) and the AOD Differences Between Nighttime and Daytime From CALIOP Observations and GEOS-Chem Simulations in 2019*

| Name | Daytime | Nighttime | Absolute difference | Relative difference |
|---|---|---|---|---|
| CALIOP | 0.321 | 0.488 | 0.167 | 51.9% |
| CONTROL | 0.382 | 0.416 | 0.034 | 8.9% |
| TEMP$_{all}$ | 0.404 | 0.389 | −0.015 | −3.7% |
| TEMP$_{rh}$ | 0.398 | 0.380 | −0.018 | −4.5% |
| WIND | 0.387 | 0.421 | 0.034 | 8.8% |

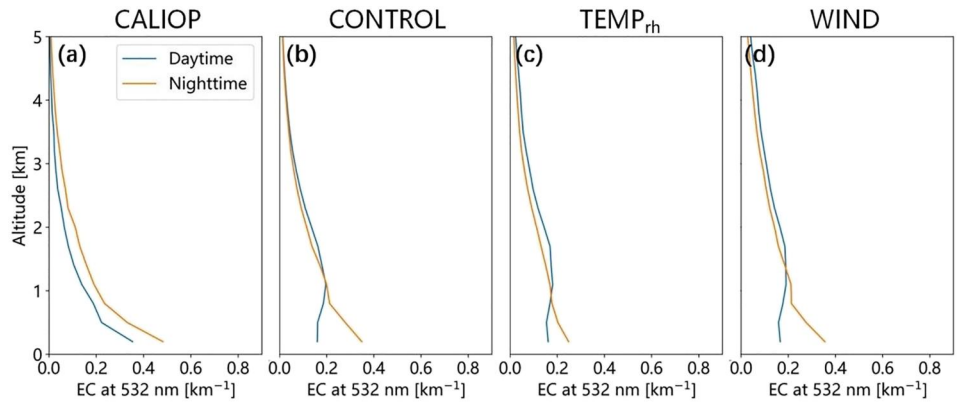


**Figure 6.** The daytime (blue line) and nighttime (orange line) Extinction Coefficient (EC) profiles at 532 nm over eastern China (boxes in Figure 2) in 2019 from CALIOP (a), CONTROL (b), $TEMP_{rh}$ (c) and WIND (d).

Chem simulations that are paired with CALIOP "clear air" samples have positive EC values, which could partly explain why the diel difference is smaller in the GEOS-Chem CONTROL run than in the CALIOP data. On the other hand, Campbell et al. (2012) and Su et al. (2020) showed that AOD in the nighttime is smaller than that in the daytime, which can be partly explained by the fact that "clear air" samples are not included in their calculation of mean AOD. Excluding the "clear air" samples in the calculation of mean AOD means small values are not included, hence will lead to a positive bias. As there are more "clear" samples at daytime than that at nighttime (Figure 10a), excluding the "clear air" samples in the calculation of mean AOD (Campbell et al., 2012; Su et al., 2020) result in a larger artificial overestimation in the daytime than that in the nighttime.

We use three approaches to analyze the impact of the difference in CALIOP "clear air" detection between daytime and nighttime on our results. The first is to set the EC to 0 ("clear air") for all nighttime retrievals whose values are smaller than the minimum daytime aerosol detection threshold of 0.067 km$^{-1}$ (Rogers et al., 2014; Toth et al., 2018), which means degrade the detection limit in the nighttime to that in the daytime (0.067 km$^{-1}$). The degraded nighttime CALIOP retrieval ability and EC profiles are shown in Figures 10a and 10b, respectively. After degrading the detection limit in the nighttime to that in the daytime, the percentages of valid CALIOP EC retrievals in the daytime and nighttime are similar to each other (Figure 10a). Compared with that AOD above 1 km in the nighttime is 0.105 larger than that at the daytime in Figure 5a, the difference decreases to 0.073 in Figures 10b and 10c. In the second method, we use AERONET AOD measurement to correct CALIPO AOD bias in the daytime. A previous global validation revealed that mean CALIOP AOD is ~80% of AERONET AOD in the daytime (Omar et al., 2013). After applying this correction factor of 0.8, the adjusted CALIOP daytime AOD comes out to 0.401 (derived from the 0.321 in Table 2 divided by 0.8). This value remains below the CALIOP nighttime AOD of 0.488, as indicated in Table 2. With the caveat that both the threshold of 0.067 km$^{-1}$ and the correction factor of 0.8 are not specifically derived for eastern China, the inferences drawn from these results are estimates rather than the most accurate determination of the CALIOP day-night AOD bias in eastern China. In the third method, we use the estimation of Undetected Layer AOD (ULA) from Kim et al. (2017) to bound the bias of diel AOD difference caused by the diurnal variation in ULA. Kim et al. (2017) estimated that ULA is $0.036 \pm 0.066$ and $0.025 \pm 0.021$ at daytime and nighttime, respectively. As a back-of-the-envelope calculation, we add the daytime ULA upper limit ($0.036 + 0.066 = 0.102$) and nighttime ULA lower limit ($0.025 - 0.021 = 0.004$) to CALIOP AODs at daytime (0.321) and nighttime (0.488), respectively. With this estimation, the CALIOP AOD at nighttime becomes 0.492, which is still 16.3% larger than 0.423 at daytime.

In the CALIOP EC retrieval algorithm, each aerosol type has a lidar ratio, and the uncertainties associated with the selection of lidar ratio (aerosol type) cannot be omitted. For one thing, under the same condition, the diurnal depolarization due to solar background contamination could lead to a difference in aerosol type (lidar ratio) classification between daytime and nighttime. For another thing, lidar ratio grows with relative humidity increases, which can lead to an underestimate of EC or AOD under the high relative humidity condition (Zhao et al., 2017). As relative humidity is higher in the nighttime than that in the daytime, the uncertainty of lidar ratio may lead to more underestimate of AOD in the nighttime than daytime. This artifact does not contribute to that CALIOP AOD in the nighttime is larger than that in daytime, but attenuates it. In inclusion, it is important to

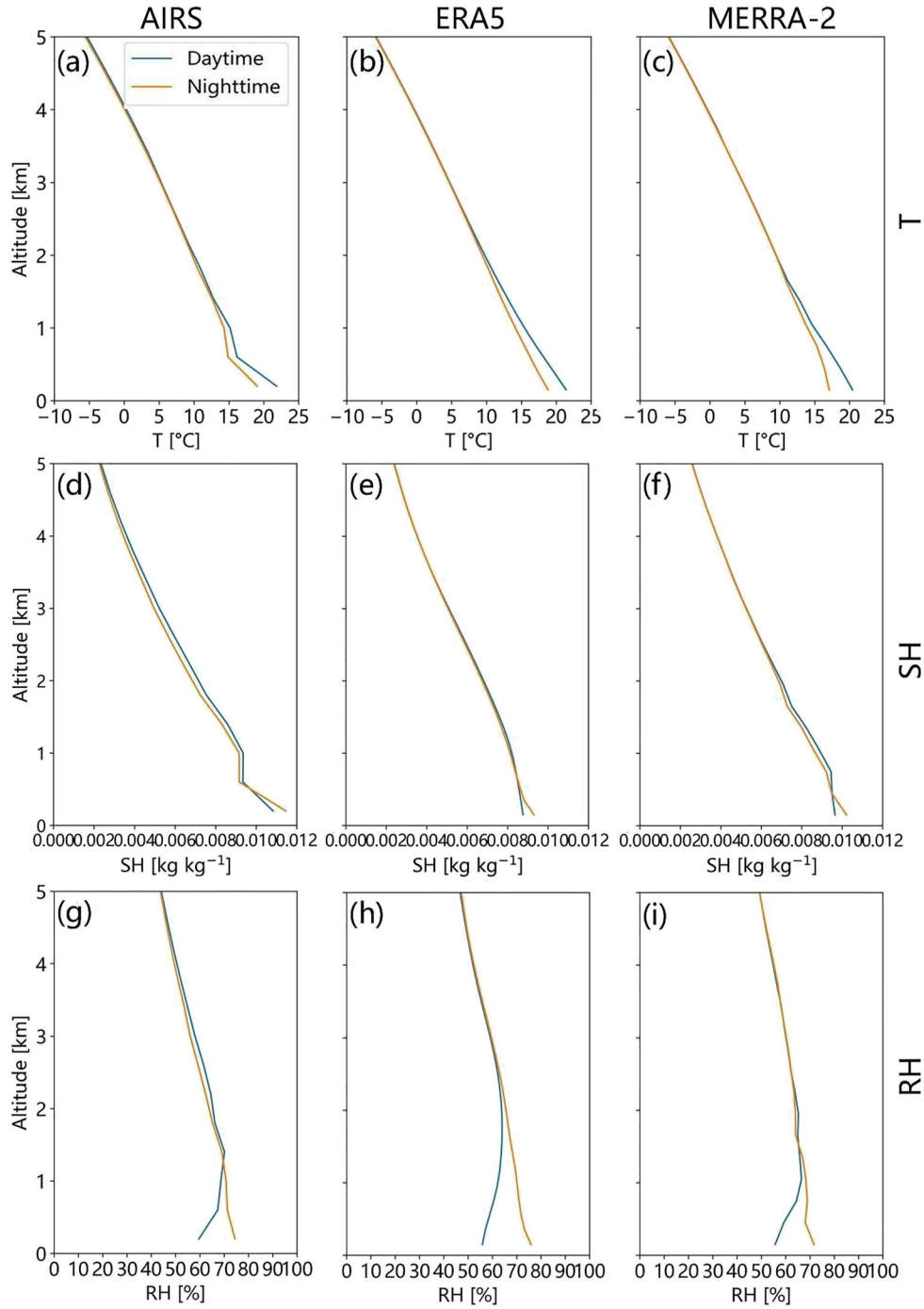


**Figure 7.** The temperature (first row), specific humidity (second row), and relative humidity (third row) profiles in daytime (blue line) and nighttime (orange line) over eastern China in 2019 from AIRS (first column), ERA5 (second column), and MERRA-2 (third column).

recognize the EC profile difference between daytime and nighttime is a combination of natural diurnal variability and artifact (Huang et al., 2013). Therefore, this study uses GEOS-Chem model simulation to estimate the natural diurnal variability and compare it with diel difference reported by CALIOP.

We further corroborate the enhancement of AOD at nighttime over eastern China through ground observations. There is one AERONET site (Beijing_CAMS) over eastern China that observed AOD at both daytime and

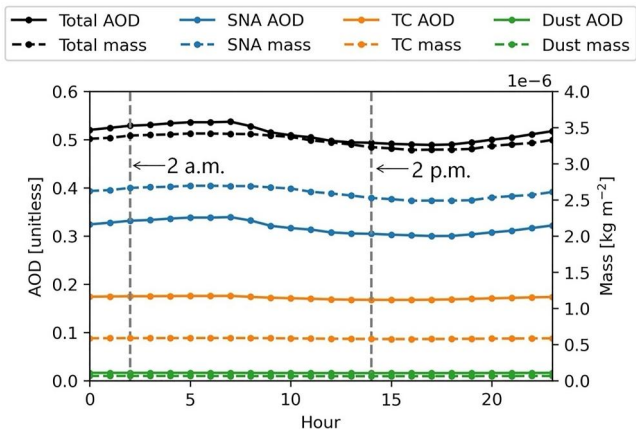


**Figure 8.** Diurnal variations in total, Sulfate-Nitrate-Ammonium (SNA), Total Carbon (TC), and dust columnar dry mass concentrations (dashed line) and optical depths (solid line) from the CONTROL simulation over eastern China in 2019.

nighttime in 2019 (The location is shown in Figure S6 in Supporting Information S1). For the observations from the site, we select only the data on the days when both daytime and nighttime AOD measurements are available. Under this criterion, there are 111 matched days. The average nighttime AOD is 0.33, which is 7.5% larger than the corresponding average daytime AOD. The difference is statistically significant with $p < 0.01$. The relative difference is much smaller than that derived from CALIOP data but is comparable to the GEOS-Chem CONTROL simulation. The daytime and nighttime AERONET AOD uncertainties are 0.01–0.02 (Giles et al., 2019) and 0.012–0.022 (Barreto et al., 2019), respectively. To decrease the impact of observational uncertainty on the analysis, only the days with the absolute value of the difference between daytime and nighttime AOD larger than 0.042 (0.02 for daytime plus 0.022 for nighttime) are counted, and there are 78 days meeting this criterion. Under these conditions, the average nighttime AOD is 0.468, which is 25.8% larger than 0.372 of the daytime AOD. The difference is also statistically significant with $p < 0.05$. Hence, AERONET data suggests that the large diel AOD difference derived from CALIOP data can be in part attributed to the particle hygroscopic growth (as counted in GEOS-Chem simulation), although its portion caused by CALIOP artifacts can also be significant and should be further investigated together with the representativeness of one AERONET site for the whole study region and year.

### 4.2. Emissions

In the GEOS-Chem simulations, daily anthropogenic NO emissions are allocated to every hour according to the diurnal profile (Figure 1), and other daily anthropogenic emissions are allocated evenly. This configuration is in part a result of consideration that gas-to-particle conversion from NO to nitrate is the largest contributor to aerosol mass throughout the day and night (Figure S7a in Supporting Information S1). Although the emission strength at nighttime is smaller than that in the daytime in CONTROL (Figure 1), the simulation result shows that nighttime AOD is 8.9% larger than that in the daytime. If aerosol hygroscopic grow is not included in the CONTROL run, AOD at nighttime is 2.0% smaller than that in the daytime. Furthermore, we conducted another GEOS-Chem simulation (named as EMI_NO) in which anthropogenic NO emissions are allocated evenly. The relative AOD difference between nighttime and daytime changes from 8.9% to 10.3%. If hygroscopic growth is not considered, the relative difference is only 2.0%. Thus, if we want to obtain a simulation result in which AOD at nighttime is larger than that in the daytime without aerosol hygroscopic growth, nighttime emissions will have to be increased significantly to rival the daytime emissions, which is not realistic. Assuming all other factors are equal, the lower emissions at night alone cannot explain the higher nighttime AOD.

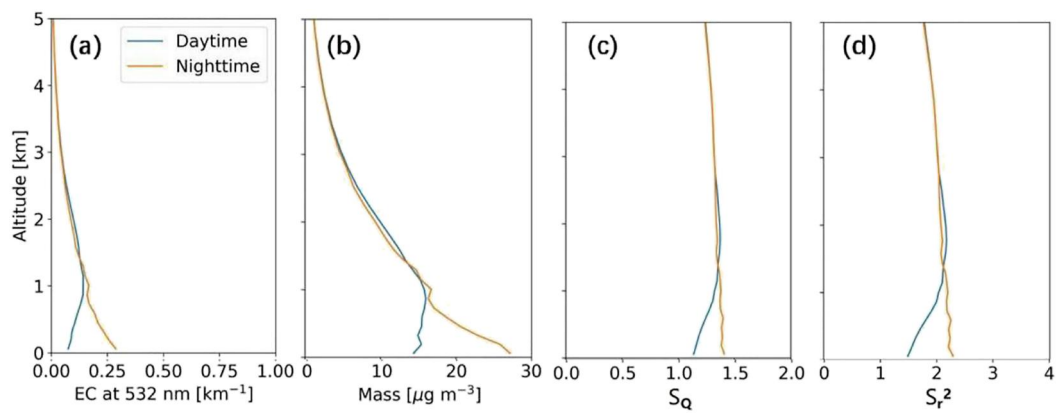


**Figure 9.** Daytime (blue line) and nighttime (orange line) SNA Extinction Coefficient (EC) profile at 532 nm (a), dry mass profile (b), extinction efficiency scale factor profile (c) and the square of SNA radius growth factor profile (d) over eastern China (boxes in Figure 2) in 2019 from CONTROL.

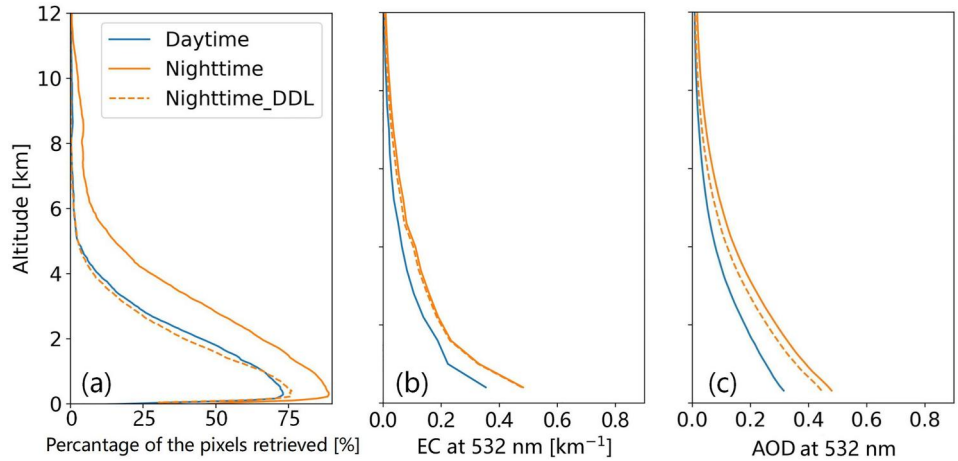


**Figure 10.** (a) Percentage of pixels valid for aerosol Extinction Coefficient (EC) to the total from the CALIOP level-2 product over eastern China in 2019 in the daytime and nighttime. For nighttime, orange solid line is plotted with all valid retrievals, while orange dashed line shows the results after assuming any EC values smaller than 0.067 km$^{-1}$ are "clear air" (denoted as Nighttime_DDL, or degradation of detection limit). (b) EC profiles at 532 nm over eastern China in 2019 from CALIOP in the daytime and nighttime. For nighttime, orange solid line indicates the EC profiles with consideration of all valid retrievals, while orange dashed line shows the results after setting any EC values smaller than 0.067 km$^{-1}$ to zero in the spatiotemporal averaging. (c) AOD that is calculated through (b) and above various altitudes.

To further evaluate the impact of diurnal variation of other emissions on AOD diurnal variation, we conduct the EMI_SBO simulation in which NO, $SO_2$, BC, and OC emissions (e.g., major contributor to aerosol mass and AOD, as shown in Figure S7 in Supporting Information S1) are allocated to every hour according to the profiles in Figure 1 and Figure S8 in Supporting Information S1 and all other settings are the same as CONTROL. In EMI_SBO, nighttime AOD is 0.407, which is still 6.0% larger than the daytime AOD. This difference is statistically significant with $p < 0.01$. Compared with the relative difference of −4.5% in $TEMP_{rh}$, this also demonstrate the importance of hydroscopic growth in the nighttime.

## 5. Conclusions and Future Studies

The CALIOP product observes that the yearly AOD over eastern China at nighttime is larger than that in the daytime from 2007 to 2019. To quantify the factors in the larger nighttime AOD, we use the GEOS-Chem chemistry transport model to simulate AOD and Extinction Coefficient (EC) over eastern China in 2019, when the largest daytime-and-nighttime relative difference in AOD exists. We also conduct uncertainty analysis regarding CALIOP extinction coefficient data quality and sampling difference between daytime and nighttime.

The CALIOP AOD over eastern China at nighttime is 51.9% larger than that in the daytime in 2019. The GEOS-Chem CONTROL simulation captures this phenomenon, although the relative difference between nighttime and daytime is only 8.9%. CALIOP shows a larger relative difference than GEOS-Chem partly because more aerosols layers are detected at nighttime than during the daytime in the CALIOP EC retrieving algorithm, which is especially evident below 5 km. When we focus solely on aerosols below 1 km, the GEOS-Chem AOD in the nighttime time is 58.5% larger than that in the daytime, which is comparable to 41.3% from CALIOP.

After counting the difference in CALIOP detection limit between daytime and nighttime, CALIOP AOD is still larger at night than in the daytime by 41.4%. This result in combination with the analysis of AERONET data showing significantly larger AOD at night than in the daytime suggest there are physical reasons and processes contributing to the larger AOD at night. Subsequently, three GEOS-Chem sensitivity simulations are conducted to quantify the impacts of transport, temperature, and hygroscopic growth on the larger nighttime AOD. In the WIND simulation, nighttime wind is replaced with daytime wind, but AOD is still 8.8% larger than daytime, which is comparable to the 8.9% in the CONTROL simulation. In the $TEMP_{all}$ simulation, nighttime temperature is replaced with daytime temperature, and nighttime AOD is 3.7% smaller than that in the daytime. Therefore, the lower nighttime temperature has important contributions to the larger nighttime AOD. To further sperate the impact of chemistry and hygroscopic growth, the $TEMP_{rh}$ simulation is conducted, in which only the nighttime

temperature used for calculating the relative humidity related to aerosol hygroscopic growth is replaced with daytime temperature. The simulated nighttime AOD difference between $TEMP_{all}$ and $TEMP_{rh}$ is only 0.009, indicating that the low nighttime temperature enhances nighttime AOD mainly through hygroscopic growth. Furthermore, an analysis of the hourly species and AOD also supports the importance of hygroscopic growth in contributing to the large nighttime AOD. Overall, we found that the aerosol hygroscopic growth leads to an increase in AOD by 0.174 at night, which in turn change the difference in AOD between nighttime and daytime from −0.05 (without hygroscopic growth) to 0.034.

This study reveals that the larger AOD at nighttime over eastern China than that in the daytime is primarily due to greater hygroscopic growth at night. This result suggests the importance of nighttime observations of aerosol optical depth and vertical profile of extinctions for constraining the fidelity in our model simulations of aerosol life cycle that affect aerosol radiative effects and air quality at both daytime and nighttime. Future studies, likely with synergistic use of satellite, model, and field observation data, are needed to understand composition-dependent hygroscopic growth for aerosols by aerosol species at different seasonal, diurnal, and regional scale. Until then, as CALIOP, the chief senor used for studying nighttime aerosols globally from space in the last ∼17 years, was decommissioned in August 2023, an equally emergent need is the routine measurements of nighttime aerosols from space (Wang et al., 2016; Yorks et al., 2023; Zhou et al., 2021) for understanding aerosol transport, aerosol optical properties, and surface $PM_{2.5}$ at night.

## Data Availability Statement

The CALIOP data were from NASA (2023b). The AIRS data were from NASA (2023a). The ERA5 data were from ECMWF (2023). The GEOS-Chem model was from GEOS-Chem Support Team (2023). Figures were made with Matplotlib version 3.2.1 (Caswell et al., 2020; Hunter, 2007).

**Acknowledgments**
This research was supported by the National Natural Science Foundation of China (Grant 42201409). Jun Wang and Meng Zhou's participation was made possible via in-kind support from the University of Iowa.

## References

Aumann, H. H., Chahine, M. T., Gautier, C., Goldberg, M. D., Kalnay, E., McMillin, L. M., et al. (2003). AIRS/AMSU/HSB on the Aqua mission: Design, science objectives, data products, and processing systems. *IEEE Transactions on Geoscience and Remote Sensing*, *41*(2), 253–264. https://doi.org/10.1109/tgrs.2002.808356

Balmes, K. A., Fu, Q., & Thorsen, T. J. (2021). The diurnal variation of the aerosol optical depth at the ARM SGP site. *Earth and Space Science*, *8*(10), e2021EA001852. https://doi.org/10.1029/2021ea001852

Barreto, A., Román, R., Cuevas, E., Pérez-Ramírez, D., Berjón, A. J., Kouremeti, N., et al. (2019). Evaluation of night-time aerosols measurements and lunar irradiance models in the frame of the first multi-instrument nocturnal intercomparison campaign. *Atmospheric Environment*, *202*, 190–211. https://doi.org/10.1016/j.atmosenv.2019.01.006

Bey, I., Jacob, D. J., Yantosca, R. M., Logan, J. A., Field, B. D., Fiore, A. M., et al. (2001). Global modeling of tropospheric chemistry with assimilated meteorology: Model description and evaluation. *Journal of Geophysical Research*, *106*(D19), 23073–23095. https://doi.org/10.1029/2001jd000807

Burnett, R. T., Pope, C. A., Ezzati, M., Olives, C., Lim, S. S., Mehta, S., et al. (2014). An integrated risk function for estimating the global burden of disease attributable to ambient fine particulate matter exposure. *Environmental Health Perspectives*, *122*(4), 397–403. https://doi.org/10.1289/ehp.1307049

Campbell, J. R., Tackett, J. L., Reid, J. S., Zhang, J., Curtis, C. A., Hyer, E. J., et al. (2012). Evaluating nighttime CALIOP 0.532 μm aerosol optical depth and extinction coefficient retrievals. *Atmospheric Measurement Techniques*, *5*(9), 2143–2160. https://doi.org/10.5194/amt-5-2143-2012

Caswell, T. A., Droettboom, M., Lee, A., Hunter, J., Firing, E., Sales De Andrade, E., et al. (2020). Matplotlib/matplotlib: Rel: V3.2.1 Zenodo. [Software]. https://doi.org/10.5281/zenodo.3714460

Crippa, M., Solazzo, E., Huang, G., Guizzardi, D., Koffi, E., Muntean, M., et al. (2020). High resolution temporal profiles in the emissions database for global atmospheric research. *Scientific Data*, *7*(1), 121. https://doi.org/10.1038/s41597-020-0462-2

ECMWF (2023). ERA5 dataset. [Dataset]. https://cds.climate.copernicus.eu/. last accessed 2 April 2023.

Fairlie, T. D., Jacob, D. J., & Park, R. J. (2007). The impact of transpacific transport of mineral dust in the United States. *Atmospheric Environment*, *41*(6), 1251–1266. https://doi.org/10.1016/j.atmosenv.2006.09.048

Fu, D., Xia, X., Duan, M., Zhang, X., Li, X., Wang, J., & Liu, J. (2018). Mapping nighttime $PM_{2.5}$ from VIIRS DNB using a linear mixed-effect model. *Atmospheric Environment*, *178*, 214–222. https://doi.org/10.1016/j.atmosenv.2018.02.001

Gasparini, B., McGraw, Z., Storelvmo, T., & Lohmann, U. (2020). To what extent can cirrus cloud seeding counteract global warming? *Environmental Research Letters*, *15*(5), 054002. https://doi.org/10.1088/1748-9326/ab71a3

Ge, J. M., Su, J., Ackerman, T. P., Fu, Q., Huang, J. P., & Shi, J. S. (2010). Dust aerosol optical properties retrieval and radiative forcing over northwestern China during the 2008 China-U.S. joint field experiment. *Journal of Geophysical Research*, *115*(D7). https://doi.org/10.1029/2009jd013263

Gelaro, R., McCarty, W., Suárez, M. J., Todling, R., Molod, A., Takacs, L., et al. (2017). The Modern-Era Retrospective analysis for research and Applications, version 2 (MERRA-2). *Journal of Climate*, *30*(14), 5419–5454. https://doi.org/10.1175/jcli-d-16-0758.1

GEOS-Chem Support Team. (2023). The GEOS-chem chemistry transport model. [Software]. Retrieved from https://geoschem.github.io/. last accessed 2 April 2023.

Giles, D. M., Sinyuk, A., Sorokin, M. G., Schafer, J. S., Smirnov, A., Slutsker, I., et al. (2019). Advancements in the Aerosol Robotic Network (AERONET) Version 3 database – Automated near-real-time quality control algorithm with improved cloud screening for Sun photometer aerosol optical depth (AOD) measurements. *Atmospheric Measurement Techniques*, *12*(1), 169–209. https://doi.org/10.5194/amt-12-169-2019

Gui, L., Tao, M., Wang, Y., Wang, L., Chen, L., Lin, C., et al. (2022). Climatology of aerosol types and their vertical distribution over East Asia based on CALIPSO lidar measurements. *International Journal of Climatology*, *42*(11), 6042–6054. https://doi.org/10.1002/joc.7599

Haywood, J., & Boucher, O. (2000). Estimates of the direct and indirect radiative forcing due to tropospheric aerosols: A review. *Reviews of Geophysics*, *38*(4), 513–543. https://doi.org/10.1029/1999rg000078

Hersbach, H., Bell, B., Berrisford, P., Hirahara, S., Horányi, A., Muñoz-Sabater, J., et al. (2020). The ERA5 global reanalysis. *Quarterly Journal of the Royal Meteorological Society*, *146*(730), 1999–2049. https://doi.org/10.1002/qj.3803

Huang, L., Jiang, J. H., Tackett, J. L., Su, H., & Fu, R. (2013). Seasonal and diurnal variations of aerosol extinction profile and type distribution from CALIPSO 5-year observations. *Journal of Geophysical Research: Atmospheres*, *118*(10), 4572–4596. https://doi.org/10.1002/jgrd.50407

Hunter, J. D. (2007). Matplotlib: A 2D graphics environment [Software]. *Computing in Science and Engineering*, *9*(3), 90–95. https://doi.org/10.1109/mcse.2007.55

Jackson, L. S., Crook, J. A., & Forster, P. M. (2016). An intensified hydrological cycle in the simulation of geoengineering by cirrus cloud thinning using ice crystal fall speed changes. *Journal of Geophysical Research: Atmospheres*, *121*(12), 6822–6840. https://doi.org/10.1002/2015jd024304

Jia, H., Ma, X., Yu, F., & Quaas, J. (2021). Significant underestimation of radiative forcing by aerosol–cloud interactions derived from satellite-based methods. *Nature Communications*, *12*(1), 3649. https://doi.org/10.1038/s41467-021-23888-1

Kim, M.-H., Omar, A. H., Vaughan, M. A., Winker, D. M., Trepte, C. R., Hu, Y., et al. (2017). Quantifying the low bias of CALIPSO's column aerosol optical depth due to undetected aerosol layers. *Journal of Geophysical Research: Atmospheres*, *122*(2), 1098–1113. https://doi.org/10.1002/2016jd025797

Kittaka, C., Winker, D. M., Vaughan, M. A., Omar, A., & Remer, L. A. (2011). Intercomparison of column aerosol optical depths from CALIPSO and MODIS-Aqua. *Atmospheric Measurement Techniques*, *4*(2), 131–141. https://doi.org/10.5194/amt-4-131-2011

Lee, C. J., Martin, R. V., Henze, D. K., Brauer, M., Cohen, A., & Donkelaar, A. v. (2015). Response of global particulate-matter-related mortality to changes in local precursor emissions. *Environmental Science and Technology*, *49*(7), 4335–4344. https://doi.org/10.1021/acs.est.5b00873

Lelieveld, J., Evans, J. S., Fnais, M., Giannadaki, D., & Pozzer, A. (2015). The contribution of outdoor air pollution sources to premature mortality on a global scale. *Nature*, *525*(7569), 367–371. https://doi.org/10.1038/nature15371

Liu, J., Ding, J., Rexiding, M., Li, X., Zhang, J., Ran, S., et al. (2021). Characteristics of dust aerosols and identification of dust sources in Xinjiang, China. *Atmospheric Environment*, *262*, 118651. https://doi.org/10.1016/j.atmosenv.2021.118651

Ma, X., Bartlett, K., Harmon, K., & Yu, F. (2013). Comparison of AOD between CALIPSO and MODIS: Significant differences over major dust and biomass burning regions. *Atmospheric Measurement Techniques*, *6*(9), 2391–2401. https://doi.org/10.5194/amt-6-2391-2013

Ma, X., Yu, F., & Quaas, J. (2014). Reassessment of satellite-based estimate of aerosol climate forcing. *Journal of Geophysical Research: Atmospheres*, *119*(17), 10394–10409. https://doi.org/10.1002/2014jd021670

McDuffie, E. E., Smith, S. J., O'Rourke, P., Tibrewal, K., Venkataraman, C., Marais, E. A., et al. (2020). A global anthropogenic emission inventory of atmospheric pollutants from sector- and fuel-specific sources (1970–2017): An application of the community emissions data System (CEDS). *Earth System Science Data*, *12*(4), 3413–3442. https://doi.org/10.5194/essd-12-3413-2020

Meng, Y., Zhou, J., Wang, Z., Tang, W., Ma, J., Zhang, T., & Long, Z. (2023). Retrieval of nighttime aerosol optical depth by simultaneous consideration of artificial and natural light sources. *Science of the Total Environment*, *896*, 166354. https://doi.org/10.1016/j.scitotenv.2023.166354

Myhre, G., Shindell, D., Bréon, F.-M., Collins, W., Fuglestvedt, J., Huang, J., et al. (2013). Anthropogenic and natural radiative forcing. In T. F. Stocker, D. Qin, G.-K. Plattner, M. Tignor, S. K. Allen, J. Boschung, et al. (Eds.), *Climate change 2013: The physical science basis. Contribution of working group I to the fifth assessment Report of the intergovernmental panel on climate change* (pp. 659–740). Cambridge University Press.

NASA. (2023a). The AIRS dataset [Dataset]. Retrieved from https://disc.gsfc.nasa.gov/ (last accessed April 2, 2023)

NASA. (2023b). The CALIOP dataset. [Dataset]. Retrieved from https://www-calipso.larc.nasa.gov/. last accessed 2 April 2023.

NASA. (2023c). CALIPSO: Data user's guide - data product descriptions - lidar level 3 tropospheric aerosol profile monthly product version 4.20. Retrieved from https://www-calipso.larc.nasa.gov/resources/calipso_users_guide/data_summaries/l3/cal_lid_l3_tropospheric_apro_v4-20_desc.php. last accessed 21 December 2023.

Omar, A. H., Winker, D. M., Tackett, J. L., Giles, D. M., Kar, J., Liu, Z., et al. (2013). CALIOP and AERONET aerosol optical depth comparisons: One size fits none. *Journal of Geophysical Research: Atmospheres*, *118*(10), 4748–4766. https://doi.org/10.1002/jgrd.50330

Petrenko, M., Kahn, R., Chin, M., Soja, A., Kucsera, T., & Harshvardhan (2012). The use of satellite-measured aerosol optical depth to constrain biomass burning emissions source strength in the global model GOCART. *Journal of Geophysical Research*, *117*(D18). https://doi.org/10.1029/2012jd017870

Rogers, R. R., Vaughan, M. A., Hostetler, C. A., Burton, S. P., Ferrare, R. A., Young, S. A., et al. (2014). Looking through the haze: Evaluating the CALIPSO level 2 aerosol optical depth using airborne high spectral resolution lidar data. *Atmospheric Measurement Techniques*, *7*(12), 4317–4340. https://doi.org/10.5194/amt-7-4317-2014

Seinfeld, J. H., & Pandis, S. N. (2016). *Atmospheric chemistry and physics: From air pollution to climate change* (3rd ed.). Wiley.

Smith, C., Nicholls, Z. R. J., Armour, K., Collins, W., Forster, P., Meinshausen, M., et al. (2021). The Earth's energy budget, climate feedbacks, and climate sensitivity supplementary material. In V. Masson-Delmotte, P. Zhai, A. Pirani, S. L. Connors, C. Péan, S. Berger, et al. (Eds.), *Climate change 2021: The physical science basis. Contribution of working group I to the Sixth assessment Report of the intergovernmental panel on climate change*. Retrieved from https://www.ipcc.ch/

Su, B., Li, H., Zhang, M., Bilal, M., Wang, M., Atique, L., et al. (2020). Optical and physical characteristics of aerosol vertical layers over northeastern China. *Atmosphere*, *11*(5), 501. https://doi.org/10.3390/atmos11050501

Tackett, J. L., Winker, D. M., Getzewich, B. J., Vaughan, M. A., Young, S. A., & Kar, J. (2018). CALIPSO lidar level 3 aerosol profile product: Version 3 algorithm design. *Atmospheric Measurement Techniques*, *11*(7), 4129–4152. https://doi.org/10.5194/amt-11-4129-2018

Taylor, K. E. (2001). Summarizing multiple aspects of model performance in a single diagram. *Journal of Geophysical Research*, *106*(D7), 7183–7192. https://doi.org/10.1029/2000jd900719

Tian, B., Manning, E., Roman, J., Thrastarson, H., Fetzer, E. J., & Monarrez, Z. (2020). *AIRS version 7 level 3 product user guide*. Jet Propul- sion Laboratory California Institute of Technology Pasadena. Retrieved from https://docserver.gesdisc.eosdis.nasa.gov/public/project/AIRS/V7_L3_User_Guide.pdf

Toth, T. D., Campbell, J. R., Reid, J. S., Tackett, J. L., Vaughan, M. A., Zhang, J., & Marquis, J. W. (2018). Minimum aerosol layer detection sensitivities and their subsequent impacts on aerosol optical thickness retrievals in CALIPSO level 2 data products. *Atmospheric Measurement Techniques*, *11*(1), 499–514. https://doi.org/10.5194/amt-11-499-2018

Wang, J., Aegerter, C., Xu, X., & Szykman, J. J. (2016). Potential application of VIIRS Day/Night Band for monitoring nighttime surface PM2.5 air quality from space. *Atmospheric Environment*, *124*, 55–63. https://doi.org/10.1016/j.atmosenv.2015.11.013

Wang, J., Christopher, S. A., Nair, U. S., Reid, J. S., Prins, E. M., Szykman, J., & Hand, J. L. (2006). Mesoscale modeling of central American smoke transport to the United States: 1. "Top-down" assessment of emission strength and diurnal variation impacts. *Journal of Geophysical Research*, *111*(D5). https://doi.org/10.1029/2005jd006416

Wang, J., Hoffmann, A. A., Park, R. J., Jacob, D. J., & Martin, S. T. (2008). Global distribution of solid and aqueous sulfate aerosols: Effect of the hysteresis of particle phase transitions. *Journal of Geophysical Research*, *113*(D11), D11206. https://doi.org/10.1029/2007jd009367

Wang, J., & Martin, S. T. (2007). Satellite characterization of urban aerosols: Importance of including hygroscopicity and mixing state in the retrieval algorithms. *Journal of Geophysical Research*, *112*(D17), D17203. https://doi.org/10.1029/2006jd008078

Wang, J., Xia, X., Wang, P., & Christopher, S. A. (2004). Diurnal variability of dust aerosol optical thickness and Angström exponent over dust source regions in China. *Geophysical Research Letters*, *31*(8), L08107. https://doi.org/10.1029/2004gl019580

Wang, Y., Wang, J., Xu, X., Henze, D. K., Qu, Z., & Yang, K. (2020). Inverse modeling of $SO_2$ and $NO_x$ emissions over China using multisensor satellite data – Part 1: Formulation and sensitivity analysis. *Atmospheric Chemistry and Physics*, *20*(11), 6631–6650. https://doi.org/10.5194/acp-20-6631-2020

Wei, J., Li, Z., Lyapustin, A., Sun, L., Peng, Y., Xue, W., et al. (2021). Reconstructing 1-km-resolution high-quality $PM_{2.5}$ data records from 2000 to 2018 in China: Spatiotemporal variations and policy implications. *Remote Sensing of Environment*, *252*, 112136. https://doi.org/10.1016/j.rse.2020.112136

Wei, J., Li, Z., Pinker, R. T., Wang, J., Sun, L., Xue, W., et al. (2021). Himawari-8-derived diurnal variations in ground-level $PM_{2.5}$ pollution across China using the fast space-time Light Gradient Boosting Machine (LightGBM). *Atmospheric Chemistry and Physics*, *21*(10), 7863–7880. https://doi.org/10.5194/acp-21-7863-2021

Winker, D. M., Tackett, J. L., Getzewich, B. J., Liu, Z., Vaughan, M. A., & Rogers, R. R. (2013). The global 3-D distribution of tropospheric aerosols as characterized by CALIOP. *Atmospheric Chemistry and Physics*, *13*(6), 3345–3361. https://doi.org/10.5194/acp-13-3345-2013

Winker, D. M., Vaughan, M. A., Omar, A., Hu, Y., Powell, K. A., Liu, Z., et al. (2009). Overview of the CALIPSO mission and CALIOP data processing algorithms. *Journal of Atmospheric and Oceanic Technology*, *26*(11), 2310–2323. https://doi.org/10.1175/2009jtecha1281.1

Wu, J., Yao, F., Li, W., & Si, M. (2016). VIIRS-based remote sensing estimation of ground-level $PM_{2.5}$ concentrations in Beijing–Tianjin–Hebei: A spatiotemporal statistical model. *Remote Sensing of Environment*, *184*, 316–328. https://doi.org/10.1016/j.rse.2016.07.015

Xu, J., Han, F., Li, M., Zhang, Z., Xiaohui, D., & Wei, P. (2019). On the opposite seasonality of MODIS AOD and surface $PM_{2.5}$ over the Northern China plain. *Atmospheric Environment*, *215*, 116909. https://doi.org/10.1016/j.atmosenv.2019.116909

Xu, X., Liu, C., Wang, J., Yin, Y., & Zhu, X. (2022). Long-term multidataset direct aerosol radiative forcing and its efficiencies: Intercomparisons and uncertainties. *Atmospheric Research*, *267*, 105964. https://doi.org/10.1016/j.atmosres.2021.105964

Xu, X., Wang, J., Henze, D. K., Qu, W., & Kopacz, M. (2013). Constraints on aerosol sources using GEOS-Chem adjoint and MODIS radiances, and evaluation with multisensor (OMI, MISR) data. *Journal of Geophysical Research: Atmospheres*, *118*(12), 6396–6413. https://doi.org/10.1002/jgrd.50515

Yao, F., Si, M., Li, W., & Wu, J. (2018). A multidimensional comparison between MODIS and VIIRS AOD in estimating ground-level $PM_{2.5}$ concentrations over a heavily polluted region in China. *Science of the Total Environment*, *618*, 819–828. https://doi.org/10.1016/j.scitotenv.2017.08.209

Ye, X., Cheng, T., Li, X., & Zhu, H. (2023). Impact of satellite AOD data on top-down estimation of biomass burning particulate matter emission. *Science of the Total Environment*, *864*, 161055. https://doi.org/10.1016/j.scitotenv.2022.161055

Yorks, J. E., Wang, J., McGill, M. J., Follette-Cook, M., Nowottnick, E. P., Reid, J. S., et al. (2023). A SmallSat concept to resolve diurnal and vertical variations of aerosols, clouds, and boundary layer height. *Bulletin of the American Meteorological Society*, *104*(4), E815–E836. https://doi.org/10.1175/bams-d-21-0179.1

You, W., Zang, Z., Zhang, L., Li, Y., & Wang, W. (2016). Estimating national-scale ground-level $PM_{2.5}$ concentration in China using geographically weighted regression based on MODIS and MISR AOD. *Environmental Science and Pollution Research*, *23*(9), 8327–8338. https://doi.org/10.1007/s11356-015-6027-9

Zender, C. S., Bian, H., & Newman, D. (2003). Mineral dust entrainment and deposition (DEAD) model: Description and 1990s dust climatology. *Journal of Geophysical Research*, *108*(D14), 4416. https://doi.org/10.1029/2002jd002775

Zhang, J., Reid, J. S., Miller, S. D., Román, M., Wang, Z., Spurr, R. J. D., & Jaker, S. (2023). Sensitivity studies of nighttime top-of-atmosphere radiances from artificial light sources using a 3-D radiative transfer model for nighttime aerosol retrievals. *Atmospheric Measurement Techniques*, *16*(10), 2531–2546. https://doi.org/10.5194/amt-16-2531-2023

Zhao, G., Zhao, C., Kuang, Y., Tao, J., Tan, W., Bian, Y., et al. (2017). Impact of aerosol hygroscopic growth on retrieving aerosol extinction coefficient profiles from elastic-backscatter lidar signals. *Atmospheric Chemistry and Physics*, *17*(19), 12133–12143. https://doi.org/10.5194/acp-17-12133-2017

Zheng, B., Tong, D., Li, M., Liu, F., Hong, C., Geng, G., et al. (2018). Trends in China's anthropogenic emissions since 2010 as the consequence of clean air actions. *Atmospheric Chemistry and Physics*, *18*(19), 14095–14111. https://doi.org/10.5194/acp-18-14095-2018

Zhou, M., Wang, J., Chen, X., Xu, X., Colarco, P. R., Miller, S. D., et al. (2021). Nighttime smoke aerosol optical depth over U.S. rural areas: First retrieval from VIIRS moonlight observations. *Remote Sensing of Environment*, *267*, 112717. https://doi.org/10.1016/j.rse.2021.112717